Cement and Concrete Research 137 (2020) 106197

Contents lists available at ScienceDirect

Cement and Concrete Research

journal homepage: www.elsevier.com/locate/cemconres

Influence of multi-walled carbon nanotubes on the hydration products of ordinary Portland cement paste

Jiaxin Chen[a], Ange-Therese Akono[a,b,*]

[a] Department of Civil and Environmental Engineering, Northwestern University, 60208, USA
[b] Department of Mechanical Engineering, Northwestern University, 60208, USA

ARTICLE INFO

Keywords:
Cement nanocomposites
Multi-walled carbon nanotubes
Calcium-silicate-hydrates
Nano porosity
Fracture toughness
Statistical nanoindentation
Hydration product
Scratch testing

ABSTRACT

We elucidate the mechanisms by which multi-walled carbon nanotubes (MWCNTs) influence the microstructure, fracture behavior, and hydration of cement paste. We disperse MWCNTs using a multi-step approach that involves high-energy pre-dispersion using ultrasonic energy followed by low-energy dispersion using un-hydrated cement particles. In turn, the low-energy dispersion step involves high-shear mixing and mechanical stirring. High-resolution environmental scanning electron microscopy of cement + 0.2 wt% MWCNT, cement + 0.5 wt% MWNCT, and of cement + 1 wt% MWCNT show that MWCNTs bridge air voids, thereby refining the pore size and strengthening the C-S-H matrix. The fracture toughness increased by 9.38% with the addition of 0.2 wt% multi-walled carbon nanotubes, and by 14.06% with the addition of 0.5 wt% multi-walled carbon nanotubes and ligament bridging was the dominant toughening mechanism. Moreover, for all reinforcement levels, MWCNTs induced a conversion of low-density C-S-H into high-density C-S-H along with a drastic drop in the capillary porosity: adding 0.1–0.5 wt% MWCNT resulted in a 200% increase in the volume fraction of high-density C-S-H. Thus, our experiments show that MWCNT enhances the mechanical properties and transport properties by: (i) promoting high-density C-S-H formation, (ii) promoting calcium hydroxide formation, (iii) filling microscopic air voids, (iv) reducing the capillary porosity, (v) increasing the fraction of small gel pores (1.2–2 nm in size), and (vi) by bridging microcracks.

1. Introduction

Cement paste is an essential component of concrete. However, cement paste is inherently brittle. To improve the fracture performance and the strength properties of cement paste, many studies have focused on multi-walled carbon nanotube (MWCNT) reinforcement [1–3]. Another advantage of MWCNT cement composites is the ability to improve the durability, thermal conductivity, and boost the electrical conductivity [4–8].

Many studies have shown that MWCNT-reinforced cement displayed higher strength characteristics [9–11]. Shah et al. found that the addition of 0.048 wt% of MWCNT increases the compressive strength [10]. Xu et al. found that incorporating 0.025 wt%, 0.05 wt%, and 0.1 wt% of MWCNT into cement paste can increase compressive strength by 9.4%, 18.32%, 21.78% respectively at 7 days [12]. Zou et al. synthesized cement nanocomposites using 0.038 wt% and 0.08 wt % of 9.5 nm functionalized MWCNT. They observed that MWCNTs contribute to a significant increase in the Young's modulus, the flexural strength, and the fracture energy [13]. Falara et al. cast cement nanocomposites with 0.048 wt% and 0.08 wt% of 20–40 nm wide MWCNT [14]. After 28 days of curing, they reported an increase in the modulus of elasticity by 28.4% and 47.8% respectively. Furthermore, Shah et al. tested MWCNT-modified cement specimens with reinforcement levels 0.048 wt% and 0.08 wt% using MWCNTs with different lengths. In each instance, the modulus of elasticity was increased after 3, 7, and 28 days of curing [10]. Similarly, Konsta-Gdoutos et al. showed an enhancement in the flexural strength and elastic modulus of MWCNT-modified cement after 3, 7, and 28 days of curing [15].

Several researchers showed that the fracture performance of cement nanocomposites can be improved by the addition of MWCNTs [16–20]. Hu et al. found that incorporating 0.05 wt% and 0.1 wt% of MWCNTs with a surfactant can increase the fracture toughness by 6.27%, 9.41%; However, for a 1.0 wt% reinforcement level, they reported a decrease in fracture energy by 3.12% [16]. Wang et al. found that within a range 0.05–0.15 wt% of MWCNT reinforcement levels, and using a surfactant, 0.08 wt% was the optimum concentration for the improvement in fracture toughness [17].

Many questions remain regarding the stiffening and toughening

* Corresponding author at: Department of Civil and Environmental Engineering, Northwestern University, 60208, USA.
E-mail address: ange-therese.akono@northwestern.edu (A.-T. Akono).

https://doi.org/10.1016/j.cemconres.2020.106197
Received 31 March 2020; Received in revised form 16 July 2020; Accepted 7 August 2020
Available online 09 September 2020

mechanisms of MWCNT in cement composites. There are three main prevailing hypotheses regarding the interactions of MWCNTs with cement paste. The first hypothesis is that MWCNTs fill micropores [21–23]. The second hypothesis is that MWCNTs serve as bridges between narrow cracks. The third hypothesis is that MWCNTs accelerate CSH growth through the nucleation effect [24–28]. However, the effect of MWCNTs on cement hydration products is still under debate. Some researchers agreed that MWCNTs can promote cement hydration. They concluded that the nucleation effect of MWCNTs can accelerate the crystallization process of hydration products. Many macroscopic properties like heat release in hydration, gelling time, compressive strength, flexural strength, early-age shrinkage validate that assumption [24–27,29]. However, other studies indicated that MWCNTs do not have any significant effect on hydration products. These studies took advantages of characterization methods like X-ray diffraction, differential scanning calorimetry, scanning electron microscope, Fourier transform infrared spectroscopy, and found that MWCNTs did not affect the hydration process of cement nanocomposites [30,31].

Our research objective is to investigate the effect of multi-walled carbon nanotubes on the microstructure and on the distribution of hydration products in Portland cement. Thus, we employ grid nanoindentation, microscopic scratch testing, high resolution environmental scanning electron microscopy, and analytical methods such as X-ray powder diffraction analysis, and Fourier transform infrared spectroscopy. This paper is organized as follows. First, we introduce our synthesis procedures. Second, we describe our experimental characterization approach. Finally, we present and discuss our results.

2. Material and methods

2.1. Materials

We synthesized cement nanocomposites reinforced with multi-walled carbon nanotubes at reinforcement levels of 0.0 wt%, 0.2 wt%, 0.5 wt%, and 1.0 wt%. Table 1 presents the detailed mix design. Type I Portland was used and the water-to-cement ratio was w/c = 0.44 for all mix designs. The multi-walled carbon nanotubes were provided by CheapTubes (Cheap Tubes Inc., Grafton, VT, USA) and were characterized by an outer diameter of < 8 nm, an inside diameter of 2–5 nm, a length of 10–30 μm length, and a specific surface area of 500 m^2/g. In addition, the bulk density of the multi-walled carbon nanotubes was 0.27 g/cm^3 with a true density of 2.1 g/cm^3.

Dispersing multi-walled carbon nanotubes (MWCNT) is challenging due to the presence of Van der Waals forces that promote carbon nanotube aggregation [32–34]. We continuously dispersed multiwalled carbon nanomaterials using un-hydrated cement particles in a three step-process as shown in Fig. 1. A similar multi-step approach was recently used by Rocha and coworkers [19,35]; although, in our experiments, we extend the duration of the mixing with un-hydrated cement particles. Our first step in the synthesis process was to pre-disperse multi-walled carbon nanotubes (MWCNT) using ultrasonic energy in presence of deionized water. Ultrasonic energy was provided by an ultrasonic horn VCX 750 with a dispersion energy of 1.87 kJ per gram of multi-walled carbon nanotubes. Thus, energy levels of 8 kJ, 20 kJ, and 40 kJ were used to disperse multi-walled carbon nanotubes for reinforcement levels of 0.2 wt%, 0.5 wt%, 1.0 wt% multi-walled carbon nanotubes respectively. An ice bath was implemented to reduce the heat produced by the concentrated ultrasonic energy. The multi-walled carbon nanotubes in solution were weighted before and after dispersion and the amount of evaporated deionized water was replaced. The second step was to mix the aqueous solution of dispersed multi-walled carbon nanotubes suspension with Type I Portland Cement powder, using an IKA (IKA Works Inc., Wilmington, NC) overhead stirrer equipped with a four-bladed propeller stirrer at a speed of 400 rpm for 2 min. The resulting slurry was cast in 30-mm cylindrical sample molds sealed with polyethylene films. The third step is to use an orbital shaker with a 3-mm orbit at a speed of 100 rpm for 24 h at 22 ± 2 °C.

Table 1
Mix Design of Cement Reinforced with Multi-Walled Carbon Nanotubes (MWCNT). DIW = Deionized Water.

Specimen	CT0.0	CT0.2	CT0.5	CT1.0
MWCNT, wt%	0.0	0.2	0.5	1.0
MWCNT, g	0.00	0.14	0.35	0.69
Cement, g	69.44	69.44	69.44	69.44
DIW, g	30.56	30.56	30.56	30.56

The high shear mixing and mechanical stirring steps are inspired from a comparison of cement paste to ceramics. When mixing ceramics, high shear mixing and mechanical stirring are mechanical aids commonly used to remove defects and improve the mechanical performance. In our experiments, the high shear mixing step will promote accelerated cement hydration and a dense microstructure. Scrivener and coworkers [36] showed that a high mixing speed combined with shearing conditions will accelerate the formation and growth of calcium-silicate hydrate crystals. Moreover, the continuous mechanical stirring provides continuous mechanical energy to disrupt bundled carbon nanotubes, limit secondary aggregation, and promote and maintain a state of uniform dispersion. Gay and Sanchez [37] and Mendoza et al. [38] showed that a secondary aggregation of nanomaterial occurred within the cement matrix in the absence of continuous mechanical stirring. Thus, we employed continuous stirring to promote uniform dispersion.

Afterward, the cementitious samples were demolded and soaked in sealed containers filled with deionized water for 6 days of curing at 22 ± 2 ° C. Finally, after a total of 7 days of hydration, the cementitious samples were soaked in ethanol for another 24 h to stop cement hydration.

2.2. Methods

2.2.1. Grinding and polishing

In order to prepare specimens nanoscale testing, such as scratch testing, grid nano-indentation testing, and environmental scanning electron microscope, we derived a rigorous grinding and polishing procedure. The objective was to yield a flat and smooth surface with a low surface roughness. Firstly, samples were embedded in low-viscosity epoxy resin. Embedded samples were cut into 5-mm thick slices using a precision low speed saw Techcut 4 (ALLIED High Tech Products Inc.) with N-Decane as cutting coolant, and then mounted on 30-mm aluminum disks. For grinding, we employed silicon carbide abrasive papers with 400, 600, and 1200 grit sizes. For further polishing, we used soft woven polishing cloths combined with diamond paste with polycrystalline diamond particle sizes ranging from 3 μm down to 0.25 μm. The end of each step was determined through microstructural observation using a high-resolution Nikon optical microscope. Between each step, the specimens were rinsed in an inert oil-based solvent and cleaned using ultrasonic energy for 2 min to prevent cross-contamination.

2.2.2. Scratch testing

We conducted scratch tests to study the fracture behavior of MWCNT cement nano-composites at the microscopic level. Fig. 2 a) displays a digital photograph of our experimental set-up. In our tests, a vertical force F_V was applied, from 0.03 N to 4.00 N, to push a Rockwell C diamond scratch probe into the sample at a linear loading rate of 7.94 N/min. Meanwhile, the resulting horizontal force F_T and penetration depth d were measured using high-accuracy force and displacement transducers. The scratch length was 5 mm and 8 scratch tests were conducted per specimen. Fig. 2 b) displays representative load-depth curves for all four MWCNT nanocomposites.

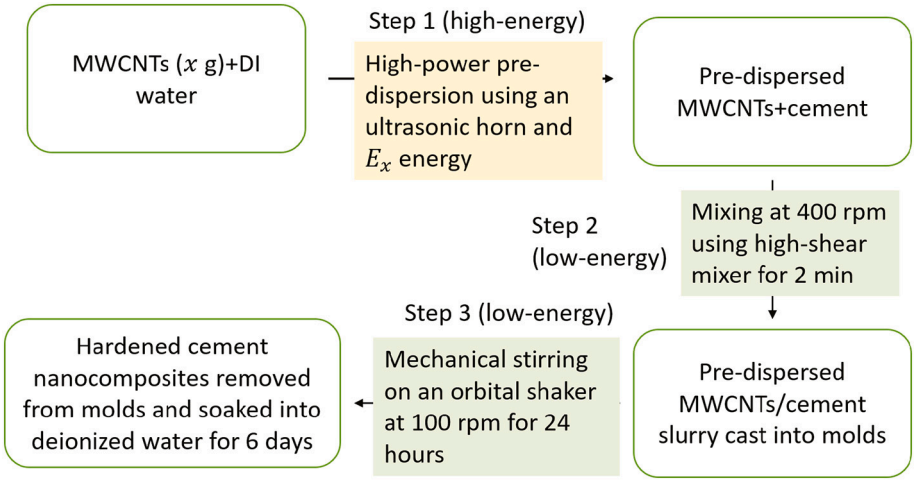

Fig. 1. Experimental protocol employed to synthesize cement nanocomposites reinforced with multi-walled carbon nanotubes.

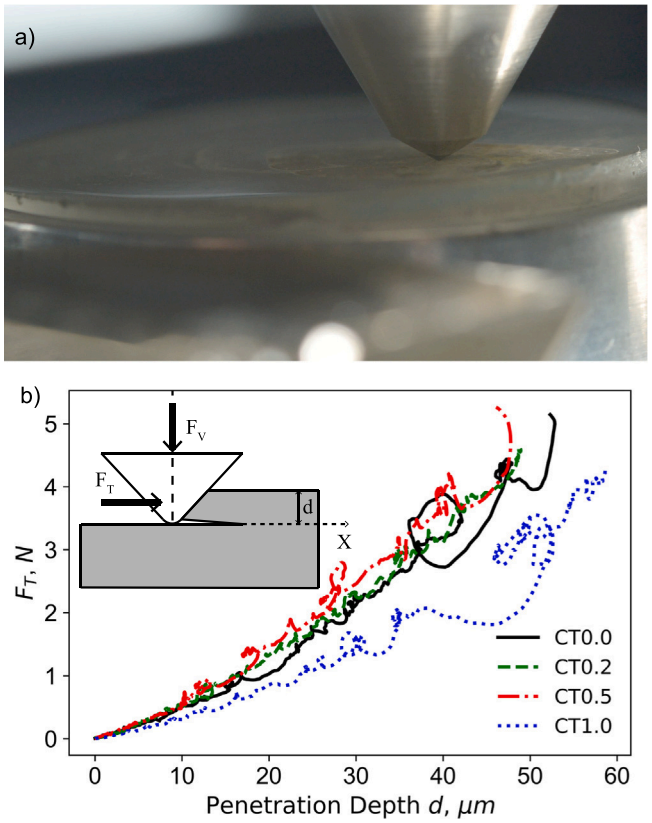

Fig. 2. a) Digital photography image of a scratch test on a composite material. Credit: Jiaxin Chen, Ange-Therese Akono, Northwestern University, 2020. b) Representative load-depth curves during scratch testing on MWCNT cement nanocomposites: CT0.0 = plain cement, CT0.2 = cement +0.2 wt% MWCNT, CT0.5 = cement +0.5 wt% MWCNT, and CT1.0 = cement +1.0 wt% MWCNT; Scratch illustration: d is the penetration depth; F_T is the horizontal force; F_V is the vertical force; X indicates the scratch path.

2.2.3. Grid nano-indentation testing

In order to capture the spatial distribution of chemomechanical phases, we conducted grid nano indentation tests. Fig. 3 a) illustrates the principle of grid nanoindentation testing. In all tests, a Berkovich diamond probe was used, which is pyramidal with an equivalent conical half-angle of $\theta = 65.27^{\circ}$.

An important question is how to design the indentation grid in terms of grid size and grid spacing. The starting point is the characteristic size of the largest heterogeneity, here the size of unhydrated clinker grains $D \propto 20\ \mu m$. The maximum indentation depth h_{max} should be an order of magnitude less than D to indent in an individual phase. Given a maximum force of 2 mN, our maximum penetration depth was in the range $h_{max} = 200 - 1700$ nm. Next, the grid size L must be at least an order of magnitude greater than D. The grid spacing ℓ must be greater than the characteristic volume probed by a single indentation ($3\ h_{max}$). Finally, a large number $N > 100$ of indents is needed to ensure the converge and accuracy of the statistical deconvolution analysis [39,40]. The following parameters satisfy all these constraints: $\ell = 25\ \mu m$, $\sqrt{N} = 21$, and $L = 500\ \mu m$.

Thus, for each specimen, a 21 × 21 grid nano-indentation was carried out with a spacing of 25 μm as shown in Fig. 3 a), spanning a total area of 500 μm × 500 μm. Furthermore, a linear increasing load P with a maximum value of 2 mN was applied at a loading/unloading rate of 4.00 mN/min with a 10 s holding phase. A representative load-penetration depth curve is presented in Fig. 3 b). For each test, the indentation hardness H and the indentation modulus M were calculated using the Oliver and Pharr's method [41–44]:

$$H = \frac{P}{A_c}; M = \frac{\sqrt{\pi}}{2}\frac{S}{\sqrt{A_c}}; S = \left.\frac{dP}{dh}\right|_{h=h_{max}} \quad (1)$$

S represents the unloading indentation stiffness. The contact area A_c can be calculated from the maximum depth h_{max} [41]. Prior to testing, the projected contact area function A_c was calibrated using fused silica as a reference material.

2.2.4. Environmental scanning electron microscopy

In order to characterize the micro-structure of cement nanocomposites reinforced with multi-walled carbon nanotubes, environmental scanning electron microscopy (ESEM) was employed using an FEI Quanta 650 environmental scanning electron microscope. Due to the low conductivity of cement materials, a low vacuum mode with an accelerating voltage of 10.00 kV was selected. a circular back-scatter detector was selected with a working distance of 10 mm, a spot size of 3.5 and an a aperture of 5. In addition, a digital image analysis routine was implemented to quantitatively identify the capillary porosity and other phases of cement nanocomposites at the microscopic scale, based on greyscale levels. To this end, the image local greyscale values were rescaled in a 0–1 range, and a histogram was displayed. Micropores and calcium hydroxide grains were identified based on image thresholding in an iterative fashion. More details regarding our digital image analysis approach are provided in the Supplementary Material.

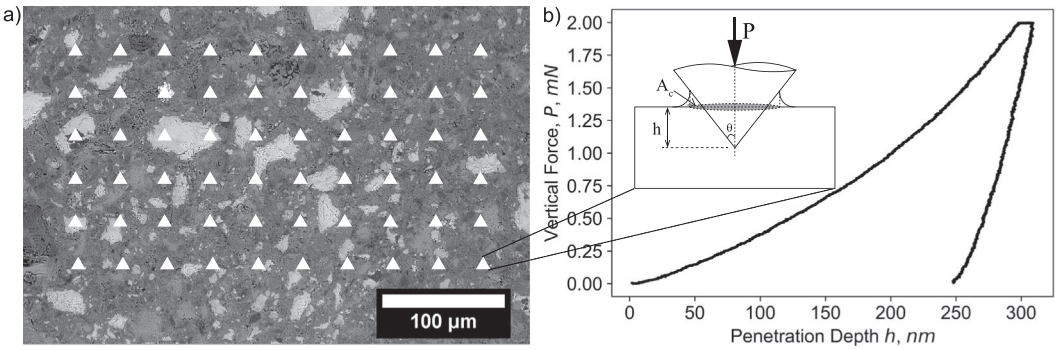

Fig. 3. a) Grid nano-indentation principle. b) Representative individual *P-h* indentation Curve *P* is the applied vertical force. *h* is the penetration depth. A_c is the contact area.

2.2.5. X-ray powder diffraction and Fourier-transform infrared spectroscopy

To characterize the chemical compositions and chemical groups of cement nanocomposites, X-ray powder diffraction (XRD) analysis and Fourier-transform infrared spectroscopy (FTIR) analysis were conducted. For X-ray powder diffraction, bulk samples were milled with ethanol using a McCrone mill to create powder specimens. A uniform final fineness of less than 1 μm was achieved. The X-ray powder diffraction tests were performed at the Jerome B.Cohen X-Ray Diffraction Facility using a Rigaku Ultima X-ray diffractometer. The tests were conducted at 40 *keV* of accessible energy and 30 mA of current with Bragg angle 2θ ranging from 10° to 60° with a step size of 0.02°. For FTIR tests, the Nicolet iS50 spectrometer (Thermo Nicolet) at the NUANCE Keck-II facility was utilized. Powder specimens were prepared using the same method as for XRD analysis. In addition, KBr pellets were prepared by pressing the mixture of powder and KBr with a weight ratio of powder sample to KBr of 1:100. Regular adsorption-transmission mode was used with a frequency range from 4000 to 400 cm^{-1} at a resolution of 4 cm^{-1}, using an average of 64 scans.

3. Theory

3.1. Multi-scale model of cement reinforced with multi-walled carbon nanotubes

We formulate a multiscale model of MWCNT-modified cement paste with three levels: C-S-H globules, C-S-H Matrix, and Cement Matrix levels as shown in Fig. 4. The classic multi-scale model of the plain ordinary Portland cement is Jenning's model [45–47], with two types of C-S-H gel morphologies: low density C-S-H and high density C-S-H. The elementary unit called globules is the same for both C-S-H gels. The globules have a radius of 2.8 nm. C-S-H consists of several globule clusters, which has six globules. Low density C-S-H was defined as an imperfectly packed structure with a packing density $\eta(LDC-S-H) = 0.64$ while high density C-S-H was defined as a closely packed structure with a packing density $\eta(HDC-S-H) = 0.74$.

In addition to Jennning's model, Ulm et al. proposed a four-level multi-scale model of concrete [48]. Level III is concrete level including cement paste, aggregates, and interfacial transition zone. Level II is cement paste level, which consists of clinker phases, calcium hydroxide crystals and macroporosity. Level I is C-S-H matrix, which has low density C-S-H, high density C-S-H, and nanoporosity. Level 0 is C-S-H solid phase including intra-globules nanoporosity and inter-globules gel porosity, and globules. Sorelli et al. [44] proposed a similar four-level scale model for ultra-high performance concrete with quartz powder at cement paste level and steel fibers at concrete level.

Our hypothesis is that multi-walled carbon nanotubes (MWCNT) will influence the microstructure at the C-S-H matrix level. As shown in Fig. 4, Level 0 is the C-S-H Globules level. The globules are at the nanometer lengthscale and consist of a monolayer of water, an interlayer of water, and C-S-H particles. The globules build up the structure of both low-density and high-density C-S-H. Level I is the C-S-H matrix with two types of C-S-H: low density C-S-H with a packing density of 64%, and high density C-S-H, with a higher packing density of 74%. We postulate that multi-walled carbon nanotubes will modify the structure of the C-S-H gel at the C-S-H matrix level by connecting C-S-H globule clusters, mainly at low density C-S-H. Thus, MWCNT act as connectors and bridges to help low density C-S-H achieve a higher packing density.

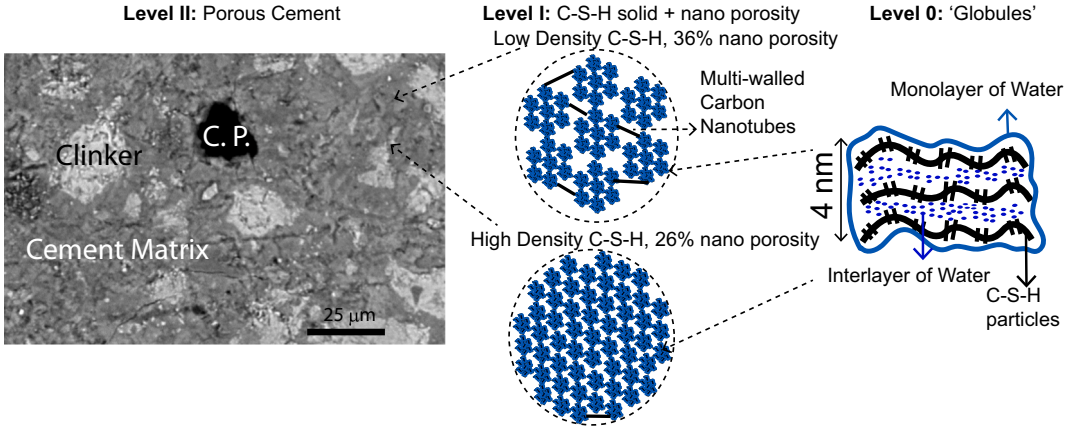

Fig. 4. Multi-scale model of cement nanocomposites reinforced with multi-walled carbon nanotubes: Level II: Porous Cement at millimeter scale including capillary pores (C. P.), anhydrous clinker (in light grey); Cement Matrix (in dark grey) including calcium hydroxide (CH) C-S-H matrix (CSH, domains); Level I: C-S-H matrix including low density C-S-H (up, low packing density), high density C-S-H (down, high packing density), nanoporosity (white), and multi-walled carbon nanotubes (black); Level 0: C-S-H 'Globules' including monolayer of water, interlayer of water, and C-S-H gel. Color online.

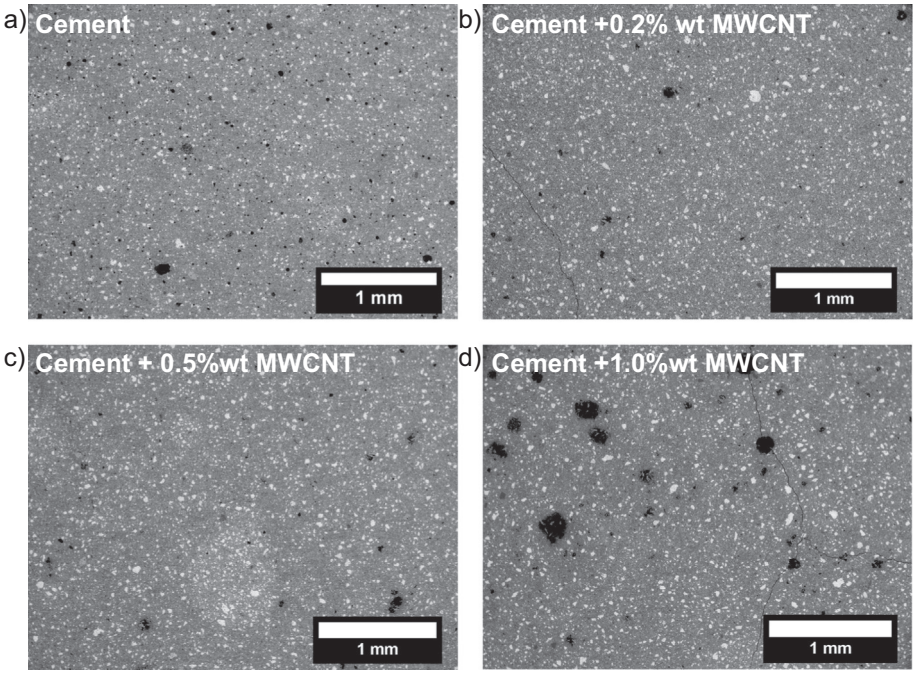

Fig. 5. a) Scanning electron microscopy images of a) Cement; b) Cement with 0.2 wt% MWCNT; c) Cement with 0.5 wt% MWCNT; d) Cement with 1.0 wt% MWCNT.

Thirdly, Level II is the Cement Matrix. Finally, Level III is the cement matrix at millimeter scale with anhydrous clinker and pores. There are four main phases in cement matrix level: capillary pores, calcium hydroxide, primary C-S-H matrix, and few anhydrous clinker.

3.2. Fracture toughness characterization and scratch testing

We used a nonlinear fracture mechanics model to calculate the fracture toughness K_c using the horizontal force F_T and penetration depth d measurements based on Akono *et.al* [49]. Assuming a semi-horizontal crack emanating from the tip of the scratch probe, the energy release rate is computed using the *J*-integral [49–52].In particular, in the asymptotic regime of a purely brittle fracture process, the model relates F_T to the scratch probe shape function *2pA* according to [49–51]:

$$\frac{F_T}{\sqrt{2pA}} = K_c \tag{2}$$

The shape function of the probe *2pA* depends on both the penetration depth and on the geometry of the scratch probe. For a spherical probe, *2pA* is a quadratic function of the penetration depth. The scratch probe shape function was calibrated prior to testing using a reference material as described in [50].

3.3. Statistical deconvolution analysis

To characterize various phases in cement nano-composites and investigate the effect of multi-walled carbon nanotubes on phase volume fraction, statistical deconvolution was implemented. This is an important method to link micro-scale and nano-scale [53], analyze the results from nano-indentation, and quantify the pore structure in cement nanocomposites.

Statistical deconvolution is a method commonly applied to decompose the overall response as a weighted contribution of individual phases [45,54–58]. For each sample, the grid nanoindentation technique yielded a distribution of $N = 441$ tests. For each single test i, the indentation hardness H_i and modulus M_i were calculated. Thus, for each sample, the entire data-set that we analyzed using the statistical deconvolution was $X_i = (M_i, H_i)_{1 \le i \le N=441}$.

By setting n as the number of material phases in the composite, each phase j is characterized by five mechanical parameters. Five parameters consist of the volume fraction f_i, the mean elastic modulus μ_j^M, the mean hardness μ_j^H, the standard deviation of the elastic modulus s_j^M, and the standard deviation of the hardness s_j^H. The theoretical cumulative distribution function $F(X_i, \mu_j^X, s_j^X)$ of a Gaussian-distributed is given by Eq. (3):

$$\begin{aligned} &F_X(X_i) = \frac{i}{N} - \frac{1}{2N}; \\ &X = (M,H); i \in [1,N] i \in [1,N] \end{aligned} \tag{3}$$

where, $X = (M, H)$, $s_j^X = (s_j^M, s_j^H)$ and $\mu_j^X = (\mu_j^M, \mu_j^H)$.

Thus, there are $5 \times n$ unknowns f_j, μ_j^M, μ_j^H, s_j^M, s_j^H with j belongs to [1,n]. Meanwhile, the theoretical value of the cumulative distribution functions $F_X(X_i)$ is given by:

$$F\left(X_i, \mu_j^X, s_j^X\right) = \frac{1}{|s_j^X|\sqrt{2\pi}} \int_{-\infty}^{X_i} exp\left(-\frac{(u-u_j^X)^2}{2\,|s_j^X|^2}\right) du \tag{4}$$

The $5n$ unknowns are determined by minimizing and optimizing the squared sum difference between the experimental cumulative distribution functions $F_X(X_i)$ and the theoretical cumulative distribution function $F(X_i, \mu_j^X, s_j^X)$, as shown in Eq. (5):

$$min \sum_{i=1}^{N} \sum_{X=(M,H)} \left[\sum_{j=1} n f_i F\left(X_i, \mu_j^X, s_j^X\right) - F_X(X_i) \right]^2 \tag{5}$$

Eq. (5) was solved by using a nonlinear constrained optimization solver in the programming language Python. In addition, we imposed two constraints. The first one is a physical constraint that the sum of the surface fractions of each phase should be equal to unity $\Sigma_{j=1}{}^n f_i = 1$. Moreover, in order to avoid overlapping of neighboring Gaussian distributions and provide sufficient contrast in properties, we enforced another set of constraints on both the elastic modulus and the hardness values as shown in Eq. (6):

$$\mu_j^X + s_j^X \le \mu_{j+1}^X - s_{j+1}^X \tag{6}$$

4. Results

4.1. Microstructure of multi-walled carbon nanotube-reinforced cement

Fig. 5 displays environmental scanning electron microscopy images of plain cement as well as MWCNT-modified cement at levels of 0.2 wt %, 0.5 wt%, and 1 wt%. For all cement-based specimens, we observe a heterogeneous microstructure consisting of capillary pores in black, C-S-H matrix in dark grey, and calcium hydroxide in light grey.

The presence of MWCNT has a positive effect on the fraction of capillary pores for low weight fractions of MWCNT. We performed a digital image analysis on SEM images at a 50× magnification level, spanning an area of 3.71 mm × 2.80 mm and we calculated the capillary porosity. We observe a downward trend for plain cement and for MWCNT weight fractions of 0.2 wt% and 0.5 wt%. The computed capillary porosity values are 0.82%, 0.132%, and 0.026%, respectively for plain cement, cement + 0.2 wt% MWCNT, and cement + 0.5 wt% MWCNT.

However, at large weight fractions, the presence of MWCNT results in an increase in the volume fraction of capillary pores and in the size of capillary pores. The computed capillary porosity value for cement + 1 wt% MWCNT is 1.465%, which represents a 79% increase compared to plain cement. Moreover, the maximum capillary pore size is 200 μm for cement + 1% MWCNT whereas it is 100 μm for plain cement, cement + 0.5 wt% MWCNT, and cement + 0.2 wt% MWCNT.

To further understand the influence of multi-walled carbon nanotubes on cement nanocomposites, high resolution scanning electron microscope was implemented as shown in Fig. 6 with magnification level 10,000–50,000 × for all three cement nanocomposites. An important question is to distinguish ettringite crystals from multi-walled carbon nanotubes. Ettringite crystals have a characteristic diameter of 2–4 μm [59]. In contrast, in the ESEM pictures, we observe rod-like features with a diameter of 100 nm and less, see Fig. 6. Thus, it is reasonable to assume that these rod-like features are MWCNTs. Multi-walled carbon nanotubes grow inside C-S-H and the growing composites appear as rod-like structures that connect grains and bridge air voids. Consequently, MWCNT contribute to a refinement of the pore size. Some MWCNT formed into bundles and we can also observe some amount of hydration product growth surrounding multi-walled carbon nanotubes. Overall, Fig. 6 supports our hypothesis of MWCNT connecting C-S-H and other hydration products. Thus, our environmental scanning electron microscopy observations support our multi-scale model shown in Fig. 4.

4.2. Fracture behavior

Therefore, we applied the scratch fracture model to understand the influence of multi-walled carbon nanotubes reinforcement on the fracture performance. Fig. 7 a) illustrates the fracture toughness calculation process on plain cement. The quantity $F_T/\sqrt{2pA}$ is displayed as a function of the scratch length X, where F_T is the horizontal force and $2pA$ is the scratch probe shape function. For low values of X, and hence low values of the penetration depths, $F_T/\sqrt{2pA}$ sharply varies. However, a convergence regime is reached for large values of X, and hence d. The convergence of $F_T/\sqrt{2pA}$ towards a horizontal asymptote reflects the convergence from ductile to brittle fracture.

Within the brittle fracture regime, Eq. (2) yields the fracture toughness, which is also the value of the asymptote. Thus, each scratch test yields a single estimate of the fracture toughness based on 1000 experimental data points; for each specimen, 8 scratch tests were conducted for statistical purposes. The fracture toughness value obtained for plain cement, 0.64 ± 0.02 MPa$\sqrt{m}$, is in agreement with values of the fracture toughness measured at the macroscopic scale on cement paste w/c = 0.44 using three-point bending tests [60] and by application of size effect upscaling methods [61]. Thus, we have a validated method to assess the fracture toughness at the microscopic scale.

Furthermore, we observe the presence of fracture processes. Fig. 7 b) shows the presence of residual groove after scratch testing. The width of the residual groove increases with the scratch path length and the penetration depth, pointing to material removal processes. Fig. 8 displays environmental scanning electron microscopy images of the residual groove in both plain cement and cement + 0.5 wt% MWCNT. We observe the presence of curved fracture surfaces. Similar fracture micro-mechanisms exist between plain cement and MWCNT-modified cement: micro-cracking, crack deflection, and crack ligament bridging.

The presence of MWCNT influences the fracture micro-mechanisms in general and the bridging process in particular. In Fig. 8, we focus on ligament bridging and we count instances of ligament bridging in both plain cement and MWCNT-modified cement for a an area spanning 200 μm × 150 μm. For plain cement, we count 6 major cracks and 10 instances of ligament bridging. Whereas, for cement + 0.5 wt% MWCNT, we count 6 major cracks and 21 ligament bridging events. Thus, MWCNT promote ligament bridging as a fracture micromechanism.

Multi-walled carbon nanotubes contribute to an increase in fracture toughness for low MWCNT weight fractions. Fig. 9 displays the evolution of the fracture toughness as a function of the weight fraction of multi-walled carbon nanotubes. The fracture toughness for plain cement, cement + 0.2 wt% MWCNT, and cement + 0.5 wt% MWCNT is respectively 0.64 ± 0.02 MPa$\sqrt{m}$, 0.70 ± 0.04 MPa$\sqrt{m}$, and 0.73 ± 0.03 MPa$\sqrt{m}$. Thus, we record a 9.4% and a 14% increase in fracture toughness for cement paste when modified with respectively 0.2 wt% and 0.5 wt% of multi-walled carbon nanotubes.

However, for high weight fractions of multi-walled carbon nanotubes, a sharp decline in fracture toughness is observed. The fracture toughness of cement + 1 wt% MWCNT is 0.49 ± 0.05 MPa, which represents a 30.6% decrease compared to plain cement. This sharp decrease in the fracture toughness can be explained by an increase in capillary porosity. This decline can also be explained by a higher level of agglomeration of MWCNTs which would inhibit their crack bridging potential.

4.3. Influence of MWCNT on the distribution of the indentation modulus

Fig. 10 displays the probability distribution functions of the indentation modulus M for both plain cement and MWCNT cement nanocomposites. The average value of the indentation modulus is 35.33 GPa for CT0.0, 45.11 GPa for CT0.2, 44.12 GPa for CT0.5, and 45.01 GPa for CT1.0. The high values of the indentation modulus are due to (i) the high speed shearing process that accelerates calcium silicate hydration [36] and (ii) due to the mechanical stirring which removes microscopic air voids while promoting a uniform dispersion of multi-walled carbon nanotubes Thus, we observed a significant increase of the stiffness in MWCNT nanocomposites showing that multi-walled carbon nanotubes contribute to stiffen cement matrices.

4.4. Calcium-silicate-hydrate phase distribution

A statistical deconvolution analysis was conducted and the probability distribution functions of the individual phases identified are shown in red dotted lines in Fig. 10. For cement hydration products, with $M < 65$ GPa, the different micro-constituents of MWCNT-modified cement were identified based on their mechanical signature. Calcium hydroxide (CH) phases had the highest values of the indentation modulus, 40.47–58.45 GPa, meanwhile capillary pores had the lowest values of the indentation modulus, less than 11 GPa. Low-density C-S-H (LD C-S-H) had indentation modulus values in the range 18.88–26.85 GPa. High-density C-S-H (HD C-S-H) had indentation values in the range 31.50–38.00 GPa. The computed values of the indentation modulus for LD C-S-H, HD C-S-H, and CH, are in agreement with experimental values reported in the scientific literature [48,62] and measured using nanoindentation experiments. The probability distribution functions for the indentation hardness are shown in the

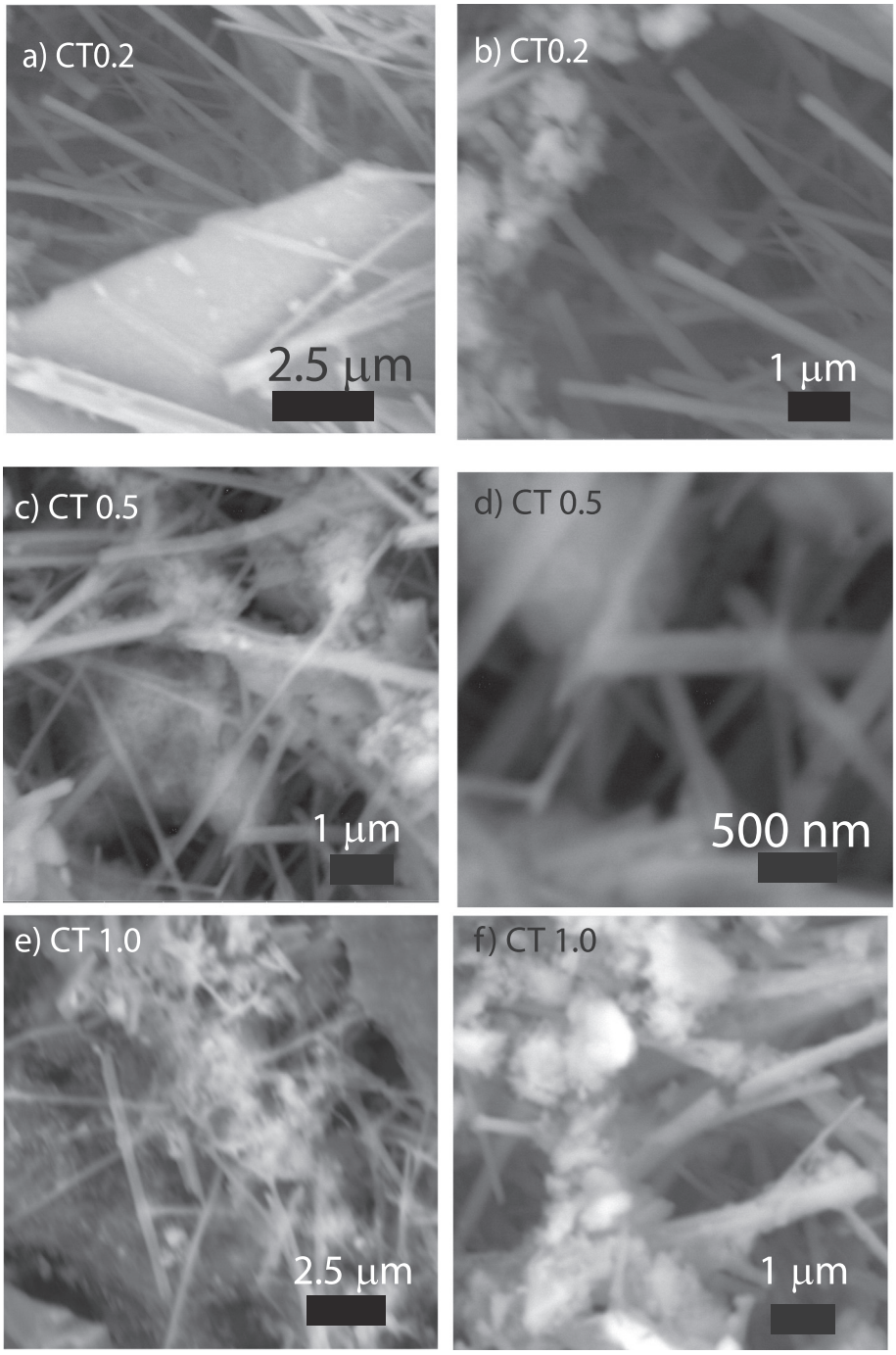

Fig. 6. Scanning electron microscopy images of MWCNT-modified cement. CT0.0 = plain cement, CT0.2 = cement + 0.2 wt% MWCNT, CT0.5 = cement + 0.5 wt% MWCNT, and CT1.0 = cement + 1.0 wt% MWCNT.

Supplementary Materials document for all composites.

Fig. 11 displays the phase distribution for plain cement and MWCNT cement nanocomposites in the (M, H) plane. Based on our multiscale model for MWCNT-modified cement, see Fig. 4, we considered four types of phases: capillary pores, low-density C-S-H, high-density C-S-H, and calcium hydroxide. By dividing the number of data points in each phase by 441 (the total number of indents), we concluded the volume fraction of each phase in Fig. 12.

The presence of MWCNT has a strong influence on the capillary porosity and on the percentage of cement hydration products. Fig. 13 displays the chemomechanical phase distribution for both plain cement and MWCNT-modified cement nanocomposites. We observe a sharp reduction in capillary pores between plain cement and MWCNT-modified cement. This reduction in capillary porosity is in agreement with the environmental scanning electron microscopy observation in Fig. 5.

Multi-walled carbon nanotubes promote an increase in high-density C-S-H and in calcium hydroxide. The volume fraction of high-density C-S-H is 22% for plain cement and is multiplied by two up to 57% and 58% for respectively cement + 0.2 wt% MWCNT and cement + 0.5 wt% MWCNT. Similarly, the volume fraction of calcium hydroxide is 16% for plain cement and that values increases to 33% and 27% for cement + 0.2 wt% MWCNT and cement + 0.5 wt% MWCNT respectively. In turn, the volume fraction of low-density C-S-H decreases with addition of MWCNT, from 20% for plain cement to 5% and 10% for cement + 0.2 wt% MWCNT and cement + 0.5 wt% MWCNT.

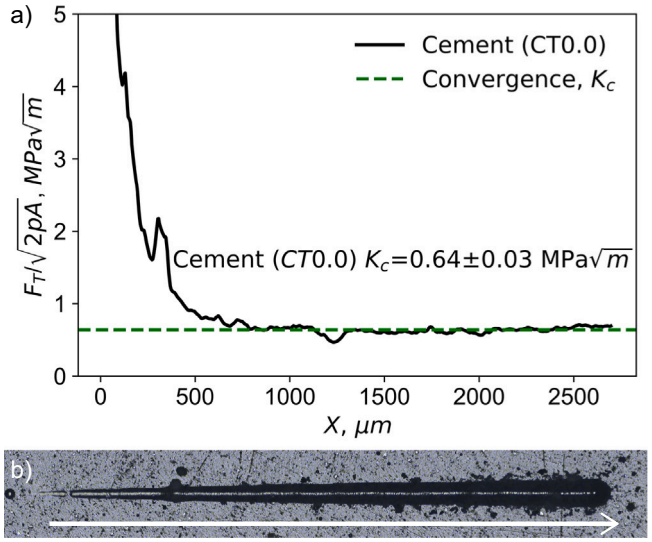

Fig. 7. a) Fracture toughness calculation: illustration on plain cement. F_T is the horizontal force, $2pA$ is the scratch probe shape function and K_c is the fracture toughness. c) Optical microscopy image of residual groove after scratch testing on plain cement specimen; the white arrow indicates the scratch direction.

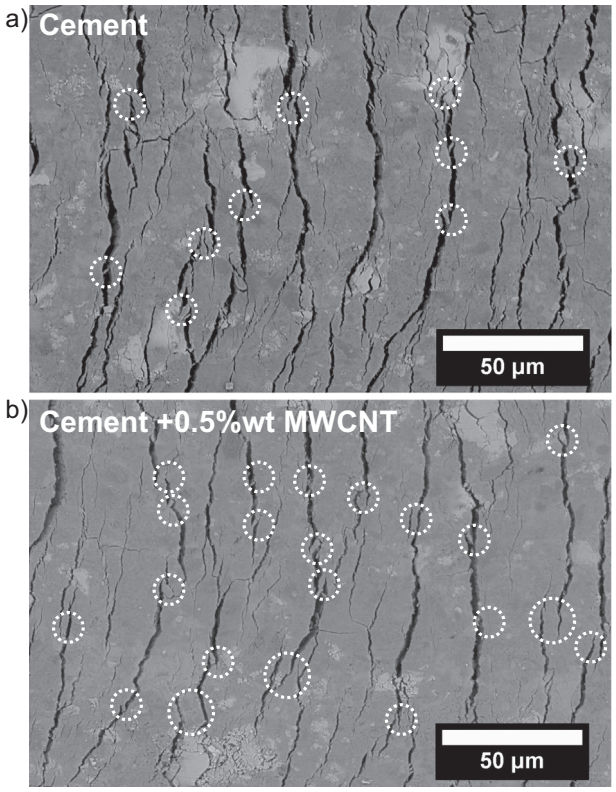

Fig. 8. Fracture micromechanisms of MWCNT cement nanocomposites. a) CT0.0; b) CT0.5, dashed circles represent bridging effects.

Multi-walled carbon nanotubes lead to an increase in C-S-H gel porosity φ. We compute the gel porosity given the volume fraction of low-density C-S-H and high-density-C-S-H according to the formula:

$$\varphi = f_{LDC-S-H}(1 - 0.64) + f_{HDC-S-H}(1 - 0.74) \quad (7)$$

where 0.64 and 0.74 are the local packing density values of respectively low-density C-S-H and high-density C-S-H [48,62]. Table 2 displays the values of the gel porosity and of the total porosity (capillary porosity and gel porosity) for both plain cement and MWCNT-modified cement

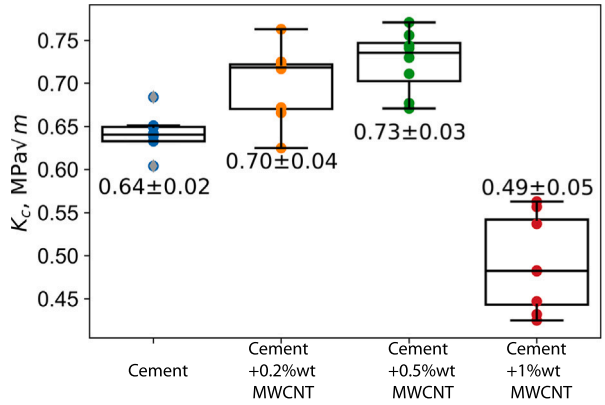

Fig. 9. Box Plot of Fracture Toughness K_c of CT0.0, CT0.2, CT0.5 and CT1.0.

paste. A surprising result is that the gel porosity of cement nanocomposites is greater than that of plain cement, with the highest increase observed for cement + 0.5 wt% MWCNT. Nevertheless, overall, the addition of multi-walled carbon nanotubes result in a decrease in the total porosity. As shown in Table 2, we observe a significant drop of the sum of capillary porosity and nanoporosity by 62.45% with the addition of 0.2 wt% multi-walled carbon nanotubes. The sum of capillary porosity and nanoporosity decreases by 56.88%, 62.56% with the addition of 0.5 wt%, 1.0 wt% respectively. Finally, the presence of multi-walled carbon nanotubes introduce a shift in the pore size distribution of MWCNT-modified cement paste, with most air voids existing as gel pores.

4.5. XRD and FTIR spectra

X-ray powder diffraction and Fourier-transform infrared spectroscopy (FTIR) were implemented to study the chemical composition and chemical groups of cement nano-composites. Figs. 13 and 14 present XRD and FTIR results of plain cement, cement + 0.2 wt% MWCNT, cement + 0.5 wt% MWCNT, and cement + 1.0 wt% MWCNT.

At low weight fractions, multi-walled carbon nanotubes lead to an increase in the calcium hydroxide (CH) orientation index. To calculate the calcium hydroxide orientation index, one must divide the CH (001) orientation peak intensity by the CH (101) orientation peak intensity [63–65]. In X-ray powder diffraction results, calcium hydroxide peaks appear at around 18.2 ° 2 θ in (001) direction at around 34.2 ° 2 θ in (101) direction. More details are shown in the Supplementary Materials document. We had and orientation index of 1.106, 1.111, 1.233, and 1.068 for plain cement, cement + 0.2 wt% MWCNT, cement + 0.5 wt% MWCNT, and cement + 1.0 wt% MWCNT respectively.

The presence of MWCNT influences the vibration frequencies of the O—H, C—O, and SiO_4^{4-} groups. At wavenumber of around 3643 cm^{-1}, the peak is referred to the stretching vibrations of O—H [33,66]. There was a slight shift to a lower wavenumber between CT0.0 and cement with multi-walled carbon nanotubes. At around 1420 cm^{-1}, which is C—O vibration bond, there was a shift to a lower frequency. At around 987 cm^{-1}, SiO_4^{-4} (asymmetric Si—O stretching) shifted towards a little lower frequency while at around 461 cm^{-1}, $_{v4}SiO_4^{-4}$ shifted towards a higher frequency when the addition of multi-walled carbon nanotubes.

5. Discussion

5.1. Stiffening mechanisms of MWCNT-modified cement

Our results show that MWCNT lead to a reduction in capillary porosity. Scanning electron microscopy images show multi-walled carbon nanotubes bridging air voids thereby reducing the pore size. Statistical deconvolution shows a neat decrease in the capillary porosity and in the total porosity. These results agree with the mercury intrusion

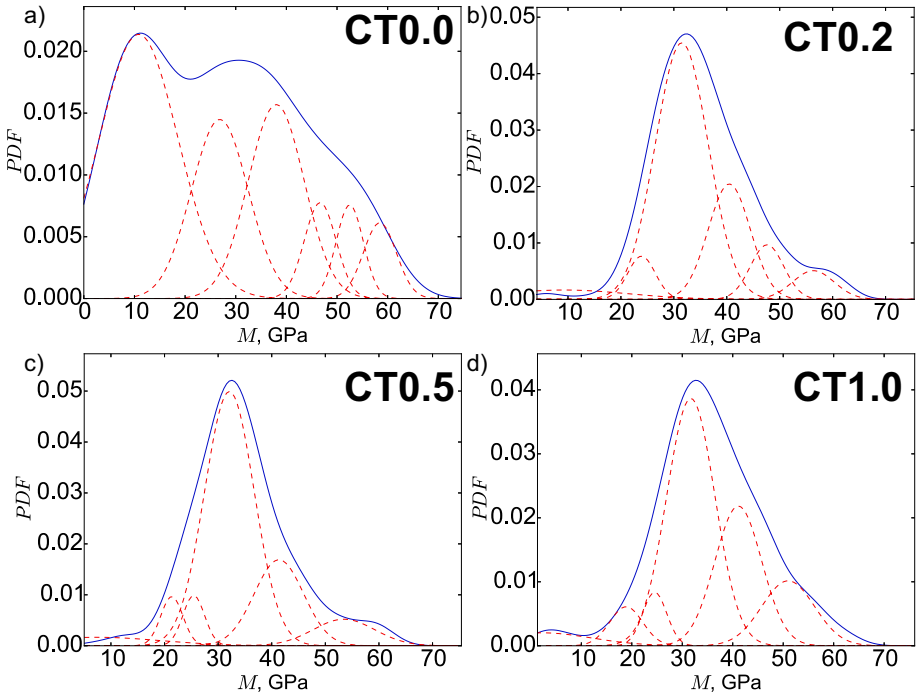

Fig. 10. Probability Distribution Functions (PDF) of the indentation modulus M for plain cement and MWCNT cement nanocomposites. a) CT0.0, b) CT0.2, c) CT0.5, d) CT1.0. (Color version online). The measured experimental probability distribution function is the solid blue line. The computed individual probability distribution functions for micro-constituents are shown using red dotted lines. (For interpretation of the references to color in this figure legend, the reader is referred to the web version of this article.)

porosimetry tests conducted by Nochaiya and Chaipanich [67,68] on cement paste w/c = 0.5 reinforced with 0.5 wt% and 1 wt% MWCNT (≈ 50 nm diameter and 500 nm length) after 28 days of hydration. They reported a decrease in the total volume intruded and in the total volume porosity. They also observed a reduction in the fraction of mesopores, in the size 6.4–80 nm. However, due to the limitations in the mercury pressure values, their method was not able to probe gel pores especially for high-density C-S-H. In high-density C-S-H, within the globules, most porosity exists in the range 1.2–2 nm [47,69]. However, within low-density C-S-H large gel mesopores exist in the 5–10 nm range. Thus, Nochaiya and Chaipanich's method [67,68] was able to probe only capillary pores and inter-LD large mesopores but not small C-S-H gel pores. Thus, the observed reduction in capillary porosity and in the volume fraction of LD C-S-H followed by an increase in HD C-S-H for cement + 0.5 wt% CNT and cement + 1 wt% CNT explains Nochaiya and Chaipanich's conclusion of a reduction in the fraction of mesopores despite an actual increase in small gel pores. A similar reduction in the fraction of mesopores in the range 25–50 nm was also reported by Hu et al. [16] on MWCNT-modified cement w/c = 0.2 with reinforcement levels of 0–0.1 wt% after 24 h of curing and by Xu et al.

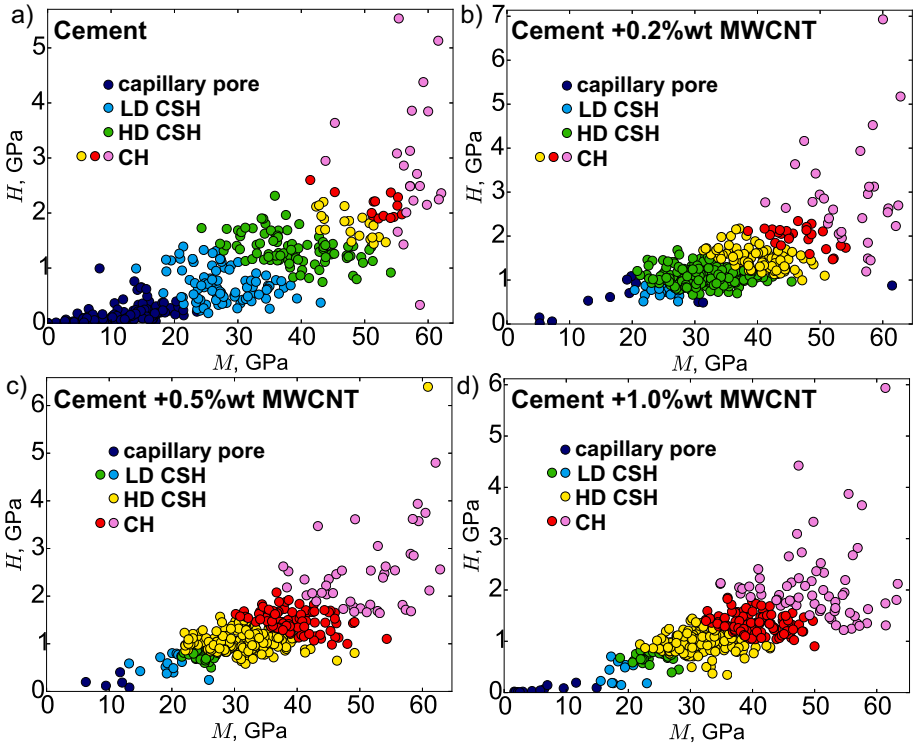

Fig. 11. Cluster analysis of indentation hardness H (GPa) and modulus M (GPa) including a) CT0.0, b) CT0.2, c) CT0.5, d) CT1.0. (Color version online).

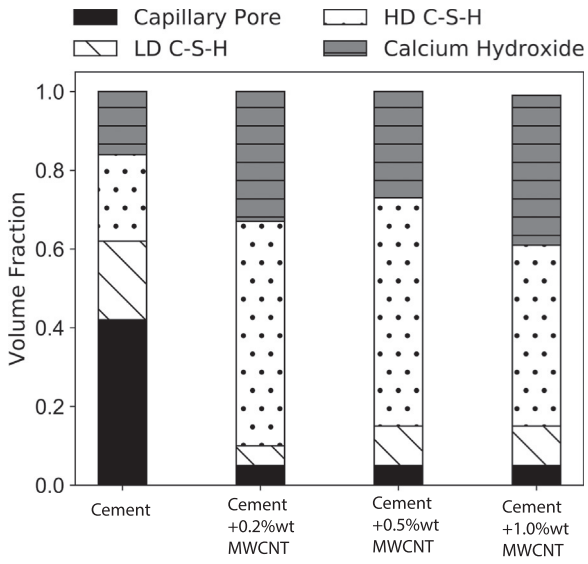

Fig. 12. Bar plot of volume fraction calculated from statistical nano-indentation for different phases including capillary pores (black), low density C-S-H white with slash, high density C-S-H (white with black dot), calcium hydroxide (grey with horizontal lines).

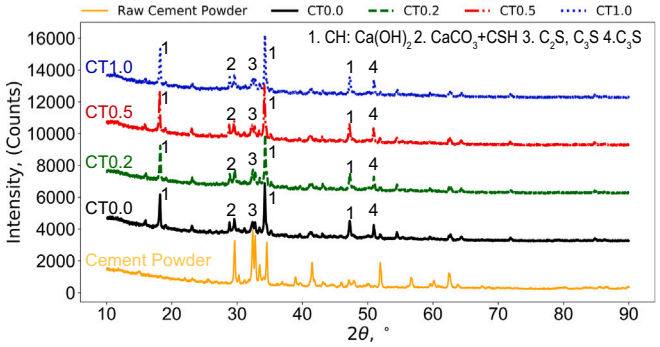

Fig. 13. X-Ray Powder Diffraction Results:CT0.0 = cement; CT0.2 = cement + 0.2 wt% MWCNT; CT0.5 = cement + 0.5 wt% MWCNT; CT1.0 = cement + 1.0 wt% MWCNT.

Table 2
Nano-porosity and Total Porosity Results.'Sum' represents'Sum of capillary porosity and nanoporosity'.

Type	Capillary Pore	LD C-S-H	HD C-S-H	Gel porosity φ	Sum
CT0.0	0.42	0.2	0.22	0.1292	0.5492
CT0.2	0.05	0.05	0.57	0.1662	0.2062
CT0.5	0.05	0.1	0.58	0.1868	0.2368
CT1.0	0.05	0.1	0.33	0.1566	0.2056

[12] on cement + 0.2 wt% MWCNT after 7 days of curing.

Our results show that MWCNT promote an increase in high-density C-S-H. Our fourier-transform infrared spectroscopy result show a shift in the spectra suggesting a change in the proportion of hydration products. At around 1420 cm^{-1}, which is C—O vibration bond, there was a shift to a lower frequency. At around 987 cm^{-1}, $SiO_4{}^{-4}$ (asymmetric Si—O stretching) shifted towards a little lower frequency while at around cm^{-1}, 461 $_{v4}SiO_4{}^{-4}$ shifted towards a higher frequency when the addition of multi-walled carbon nanotubes, which may indicate an increase in the polymerization degree of C-S-H [33]. The increase in high-density C-S-H following MWCNT cement modification had been suggested by Konsta-Gdoutos et al. [32]. They cast both short and long MWCNT-modified cement w/c = 0.3 with nano-reinforcement levels of

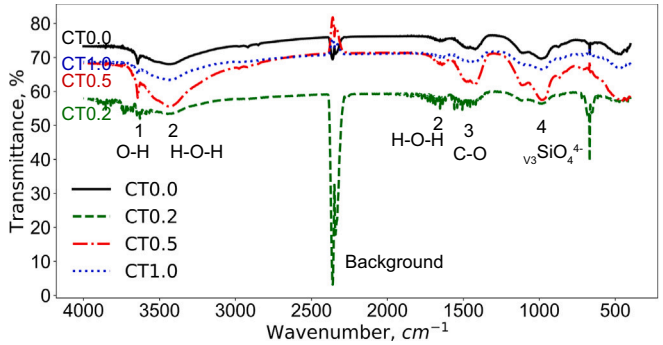

Fig. 14. FTIR Results: CT0.0 = cement; CT0.2 = cement + 0.2 wt% MWCNT; CT0.5 = cement + 0.5 wt% MWCNT; CT1.0 = cement + 1.0 wt% MWCNT, (Raw Data, no background subtraction).

0.025 wt% up to 0.1 wt%. After conducting 12 × 12 indentation grids, they noticed high probabilities values for the experimental probability function distribution of the indentation modulus in the range 20–30 GPa. In contrast, in this study we have quantitatively demonstrated that MWCNT lead to an increase in high-density C-S-H using statistical deconvolution integrated with grid nanoindentation.

Our results show that MWCNT promote calcium hydroxide crystal growth. Statistical nanoindentation shows a neat increase in calcium hydroxide volume fraction for MWCNT-modified cement. Moreover, the X-ray diffraction spectra show an increase in the calcium hydroxide orientation index for cement + xMWCNT, $X = 0.2,0.5,1.0$ wt%, which suggests that calcium hydroxide has more free space to grow [65]. This increasing for the calcium hydroxide orientation index differs from Li et al.'s results [33]. They cast muti-walled carbon nanotube cement nanocomposites with w/c = 0.3 and at reinforcement levels 0.1–0.5 wt %. They performed X-ray diffraction analysis at 24 h of hydration and reported a decrease in calcium hydroxide orientation index for cement nanocomposites. There are three possible reasons that can explain the differences between our results and Li et al.'s. Firstly, our multi-walled carbon nanotubes had a different geometry. Outer diameter of less than 8 *nm* was used in this study while they used 20–30 *nm*. In addition, we have a 500 m^2/g surface area, nearly 4 times larger surface area than theirs. Third difference is that no plasticizer was used in our study and we studied our specimens after 7 days of curing (vs. 24 h of curing in their study). In conclusion, multi-walled carbon nanotubes may provide calcium hydroxide more free growing space in cement matrix at relatively low concentrations of 0.2 wt% and 0.5 wt%.

5.2. Toughening mechanisms of MWCNT-modified cement

Our results showed that an increase in fracture toughness for multi-walled carbon nanotube reinforcement levels less or equal than 0.5 wt %. This result agrees with previous studies on MWCNT-modified cement paste [16,32] and on MWCNT-modified cement mortar [70,71]. However, in those studies researchers used macroscopic methods such as the three point bending to obtain the fracture toughness. However, so far only small reinforcement levels of multiwalled carbon nnaotubes have been considered, usually less than 0.1 wt%. In contrast, we were able to successfully cast cement + 0.5 wt% MWCNT and we observed a 14.06% increase in fracture toughness compared to plain cement.

Moreover, our fractography studies show that MWCNT promote ligament bridging. The bridging effect of MWCNT had been previously reported by many researchers such as Hu et al. [16], Abu Al-rub et al. [72], Fakhim et al. [73], Gdoutos et al. [74], by Rocha et al. [19], and Carrico et al. [75]. Herein, using microscopic scratch tests, we have shown a higher frequency of ligament bridging in MWCNT-modified cement compared to plain cement. Another MWCNT-induced toughening mechanism is the reduction in the fraction of capillary pores, which serve as potential stress concentrators.

The increase in small gel pores will contribute to improvements in mechanical and transport properties. On the one hand, an increase in high-density C-S-H will promote a high stiffness and a low creep deformation as high-density C-S-H is more dimensionally stable than low-density C-S-H [76]. Small gel pores also provide additional means to dissipate mechanical energy through nanopore rearrangement, thereby enhancing the fracture energy. On the other hand, the smaller size of gel pores in high-density C-S-H, 1.2–2 nm, will lead to a decrease of the mean pore radius and to an increase of the tortuosity (given that the gel porosity is increasing). Recent studies showed that the hydraulic conductivity of cement paste [77] is proportional to the square of the mean pore size and is inversely proportional to the square of the tortuosity. Thus, through an increase in small gel pores, MWCNT contribute to an improvement in the mechanical and transport properties.

6. Conclusions

We employ a novel approach to study the fracture behaviors, chemical composition, micro-structure and mechanical response of cementitious materials reinforced with multi-walled carbon nanotubes. We apply statistical nanoindentation integrated with grid nanoindentation along with scratch testing. We employ a multi-step approach to disperse MWCNTs involving a high-energy dispersion using ultrasonic energy followed by low-energy dispersion using un-hydrated cement particles. Below are our major findings:

- Multi-walled carbon nanotubes bridge air voids leading to a refinement of the pore structure in cement + 0.2 wt% MWCNT, cement + 0.5 wt% MWNCT, and in cement + 1 wt% MWCNT.
- Fracture toughness increased by 9.375% with the addition of 0.2 wt % multi-walled carbon nanotubes, and by 14.06% with the addition of 0.5 wt% multi-walled carbon nanotubes. The primary toughening mechanism was ligament bridging.
- Multi-walled carbon nanotubes lead to an increase in the fraction of high-density calcium silicate hydrates: adding 0.1–0.5 wt% MWCNT resulted in a 200% increase in the volume fraction of high-density C-S-H.
- Multi-walled carbon nanotubes promote calcium hydroxide growth in cement + 0.2 wt% MWCNT, cement + 0.5 wt% MWNCT, and in cement + 1 wt% MWCNT.
- Multi-walled carbon nanotubes lead to a reduction in the fraction of capillary pores and to an increase in the fraction of small C-S-H gel pores; for 0.1–0.5 wt% MWCNT more than half of the porosity exists as small gel pores (1.2–2 nm). The microstructural enhancements result in an improvement in both the mechanical and transport properties.

CRediT authorship contribution statement

Jiaxin Chen: Conceptualization, Methodology, Software, Validation, Formal analysis, Investigation, Data curation, Writing - original draft, Writing - review & editing. **Ange-Therese Akono:** Conceptualization, Methodology, Software, Validation, Formal analysis, Investigation, Resources, Data curation, Writing - review & editing, Visualization, Supervision, Project administration, Funding acquisition.

Declaration of competing interest

The authors declare that they have no known competing financial interests or personal relationships that could have appeared to influence the work reported in this paper.

Acknowledgment

This material is based upon work supported by the National Science Foundation under Grant No. CMMI 1829101. In addition, we acknowledge the Murphy's Fellowship that supported Jiaxin Chen during her Ph.D. studies in Department of Civil and Environmental Engineering at Northwestern University. This work made use of the EPIC facility of Northwestern University's NUANCE Center, which has received support from the Soft and Hybrid Nanotechnology Experimental (SHyNE) Resource (NSF ECCS-1542205); the MRSEC program (NSF DMR-1720139) at the Materials Research Center; the International Institute for Nanotechnology (IIN); the Keck Foundation; and the State of Illinois, through the IIN. This work made use of the Jerome B.Cohen X-Ray Diffraction Facility supported by the MRSEC program of the National Science Foundation (DMR-1720139) at the Materials Research Center of Northwestern University and the Soft and Hybrid Nanotechnology Experimental (SHyNE) Resource (NSF ECCS-1542205). This work made use of the Keck-II facility of Northwestern University's NUANCE Center, which has received support from the Soft and Hybrid Nanotechnology Experimental (SHyNE) Resource (NSF ECCS-1542205); the MRSEC program (NSF DMR-1720139) at the Materials Research Center; the International Institute for Nanotechnology (IIN); the Keck Foundation; and the State of Illinois, through the IIN. We acknowledge the contribution of reviewers who through their feedback have helps us to refine our thinking and improve the quality of our manuscript.

Appendix A. Supplementary data

Supplementary data to this article can be found online at https://doi.org/10.1016/j.cemconres.2020.106197.

References

[1] S. Parveen, S. Rana, R. Fangueiro, A review on nanomaterial dispersion, microstructure, and mechanical properties of carbon nanotube and nanofiber reinforced cementitious composites, J. Nanomater. 2013 (2013), https://doi.org/10.1155/2013/710175.
[2] K.M. Liew, M.F. Kai, L.W. Zhang, Carbon nanotube reinforced cementitious composites: An overview, Compos. Part A Appl. Sci. Manuf. 91 (2016) 301–323, https://doi.org/10.1016/j.compositesa.2016.10.020.
[3] F. Sanchez, K. Sobolev, Nanotechnology in concrete - A review, Constr. Build. Mater. 24 (2010) 2060–2071, https://doi.org/10.1016/j.conbuildmat.2010.03.014.
[4] O.A. Mendoza Reales, R. Dias Toledo Filho, A review on the chemical, mechanical and microstructural characterization of carbon nanotubes-cement based composites, Constr. Build. Mater. 154 (2017) 697–710, https://doi.org/10.1016/j.conbuildmat.2017.07.232.
[5] A.M. Rashad, Effect of carbon nanotubes (CNTs) on the properties of traditional cementitious materials, Constr. Build. Mater. 153 (2017) 81–101, https://doi.org/10.1016/j.conbuildmat.2017.07.089.
[6] T. Shi, Z. Li, J. Guo, H. Gong, C. Gu, Research progress on CNTs/CNFs-modified cement-based composites – A review, Constr. Build. Mater. 202 (2019) 290–307, https://doi.org/10.1016/j.conbuildmat.2019.01.024.
[7] O. Mendoza, G. Sierra, J.I. Tobón, Effect of the reagglomeration process of multi-walled carbon nanotubes dispersions on the early activity of nanosilica in cement composites, Constr. Build. Mater. 54 (2014) 550–557, https://doi.org/10.1016/j.conbuildmat.2013.12.084.
[8] R. Siddique, A. Mehta, Effect of carbon nanotubes on properties of cement mortars, Constr. Build. Mater. 50 (2014) 116–129, https://doi.org/10.1016/j.conbuildmat.2013.09.019.
[9] S. Musso, J.M. Tulliani, G. Ferro, A. Tagliaferro, Influence of carbon nanotubes structure on the mechanical behavior of cement composites, Compos. Sci. Technol. 69 (2009) 1985–1990, https://doi.org/10.1016/j.compscitech.2009.05.002.
[10] S.P. Shah, M. Konsta-Gdoutos, Z.S. Metaxa, Exploration of fracture characteristics, nanoscale properties and nanostructure of cementitious matrices with carbon nanotubes and nanofibers, Proc. 7th Int. Conf. Fract. Mech. Concr. Concr. Struct. (2010) 9–12.
[11] T.C. de Souza, G. Pinto, V.S. Cruz, M. Moura, L.O. Ladeira, J.M. Calixto, Evaluation of the rheological behavior, hydration process, and mechanical strength of Portland cement pastes produced with carbon nanotubes synthesized directly on clinker, Constr. Build. Mater. 248 (2020) 118686, , https://doi.org/10.1016/j.conbuildmat.2020.118686.
[12] S. Xu, J. Liu, Q. Li, Mechanical properties and microstructure of multi-walled carbon nanotube-reinforced cement paste, Constr. Build. Mater. 76 (2015) 16–23,

https://doi.org/10.1016/j.conbuildmat.2014.11.049.
[13] B. Zou, S.J. Chen, A.H. Korayem, F. Collins, C.M. Wang, W.H. Duan, Effect of ultrasonication energy on engineering properties of carbon nanotube reinforced cement pastes, Carbon N. Y. 85 (2015) 212–220, https://doi.org/10.1016/j.carbon.2014.12.094.
[14] G. Falara Maria, Aza Chtysoula, Oanagiotis Danoglodis, S. Konsta-Gdoutos, E. Maria, Gdoutos Emmanuel, Measurement and modeling of the elastic modulus of advanced cement based nanocomposites, Springer International Publishing Swizerland, 2015, pp. 271–276.
[15] M.S. Konsta-Gdoutos, Z.S. Metaxa, S.P. Shah, Highly dispersed carbon nanotube reinforced cement based materials, Cem. Concr. Res. 40 (2010) 1052–1059, https://doi.org/10.1016/j.cemconres.2010.02.015.
[16] Y. Hu, D. Luo, P. Li, Q. Li, G. Sun, Fracture toughness enhancement of cement paste with multi-walled carbon nanotubes, Constr. Build. Mater. 70 (2014) 332–338, https://doi.org/10.1016/j.conbuildmat.2014.07.077.
[17] B. Wang, Y. Han, S. Liu, Effect of highly dispersed carbon nanotubes on the flexural toughness of cement-based composites, Constr. Build. Mater. 46 (2013) 8–12, https://doi.org/10.1016/j.conbuildmat.2013.04.014.
[18] G. Yakovlev, G. Pervushin, I. Maeva, J. Keriene, I. Pudov, A. Shaybadullina, A. Buryanov, A. Korzhenko, S. Senkov, Modification of construction materials with multi-walled carbon nanotubes, Procedia Eng. 57 (2013) 407–413, https://doi.org/10.1016/j.proeng.2013.04.053.
[19] V. Vilela Rocha, P. Ludvig, A.C. Constancio Trindade, F. de Andrade Silva, The influence of carbon nanotubes on the fracture energy, flexural and tensile behavior of cement based composites, Constr. Build. Mater. 209 (2019) 1–8, https://doi.org/10.1016/j.conbuildmat.2019.03.003.
[20] O.A. Mendoza Reales, C. Ocampo, Y.P. Arias Jaramillo, J.C. Ochoa Botero, J.H. Quintero, E.C.C.M. Silva, R.D. Toledo Filho, Reinforcing Effect of Carbon Nanotubes/Surfactant Dispersions in Portland Cement Pastes, Adv. Civ. Eng. 2018 (2018), https://doi.org/10.1155/2018/2057940.
[21] A. Chaipanich, T. Nochaiya, W. Wongkeo, P. Torkittikul, Compressive strength and microstructure of carbon nanotubes-fly ash cement composites, Mater. Sci. Eng. A 527 (2010) 1063–1067, https://doi.org/10.1016/j.msea.2009.09.039.
[22] A. Sobolkina, V. Mechtcherine, V. Khavrus, D. Maier, M. Mende, M. Ritschel, A. Leonhardt, Dispersion of carbon nanotubes and its influence on the mechanical properties of the cement matrix, Cem. Concr. Compos. 34 (2012) 1104–1113 https://doi.org/10.1016/j.cemconcomp.2012.07.008.
[23] G.Y. Li, P.M. Wang, X. Zhao, Mechanical behavior and microstructure of cement composites incorporating surface-treated multi-walled carbon nanotubes, Carbon N. Y. 43 (2005) 1239–1245, https://doi.org/10.1016/j.carbon.2004.12.017.
[24] H. Cui, S. Yang, S.A. Memon, Development of carbon nanotube modified cement paste with microencapsulated phase-change material for structural–functional integrated application, Int. J. Mol. Sci. 16 (2015) 8027–8039, https://doi.org/10.3390/ijms16048027.
[25] J.M. Makar, J. Margeson, J. Luh, Carbon nanotube/cement composites - early results and potential applications, NRC Publ. Rec. (2005) 1–10, https://doi.org/10.1039/B910216G.
[26] J.M. Makar, G.W. Chan, Growth of cement hydration products on single-walled carbon nanotubes, J. Am. Ceram. Soc. 92 (2009) 1303–1310, https://doi.org/10.1111/j.1551-2916.2009.03055.x.
[27] S. Petrunin, V. Vaganov, V. Reshetniak, L. Zakrevskaya, Influence of carbon nanotubes on the structure formation of cement matrix, IOP Conf. Ser. Mater. Sci. Eng. 96 (2015), https://doi.org/10.1088/1757-899X/96/1/012046.
[28] P. Sikora, M. Abd Elrahman, S.Y. Chung, K. Cendrowski, E. Mijowska, D. Stephan, Mechanical and microstructural properties of cement pastes containing carbon nanotubes and carbon nanotube-silica core-shell structures, exposed to elevated temperature, Cem. Concr. Compos. 95 (2019) 193–204, https://doi.org/10.1016/j.cemconcomp.2018.11.006.
[29] O.A. Mendoza Reales, Y. Arias, C. Delgado, J. Ochoa, J. Quintero, R.D. Toledo, Surfactants as dispersants for carbon nanotubes in water: hydration of cement, Proc. 10th ACI/RILEM, Int. Conf. Cem. Mater. Altern. Bind. Sustain. Concr. (2017) 1–15.
[30] T. Shi, Y. Gao, D.J. Corr, S.P. Shah, FTIR study on early-age hydration of carbon nanotubes-modified cement-based materials, Adv. Cem. Res. 31 (2019) 353–361, https://doi.org/10.1680/jadcr.16.00167.
[31] M.S. Amin, S.M.A. El-Gamal, F.S. Hashem, Fire resistance and mechanical properties of carbon nanotubes - Clay bricks wastes (Homra) composites cement, Constr. Build. Mater. 98 (2015) 237–249, https://doi.org/10.1016/j.conbuildmat.2015.08.074.
[32] M.S. Konsta-Gdoutos, Z.S. Metaxa, S.P. Shah, Multi-scale mechanical and fracture characteristics and early-age strain capacity of high performance carbon nanotube/cement nanocomposites, Cem. Concr. Compos. 32 (2010) 110–115, https://doi.org/10.1016/j.cemconcomp.2009.10.007.
[33] Z. Li, D.J. Corr, B. Han, S.P. Shah, Investigating the effect of carbon nanotube on early age hydration of cementitious composites with isothermal calorimetry and Fourier transform infrared spectroscopy, Cem. Concr. Compos. 103513 (2020), https://doi.org/10.1016/j.cemconcomp.2020.103513.
[34] S.P. Shah, M.S. Konsta-Gdoutos, Z.S. Metaxa, Highly-dspersed carbon nanotube-reinforced cement-based materlals, United States Patent 9,365,456 B2, 2016.
[35] V.V. Rocha, P. Ludvig, A.C.C. Trindade, F. Silva, The influence of carbon nanotubes on the fracture energy, flexural and tensile behavior of cement based composites, Constr. Build. Mater. 209 (2019) 1–8.
[36] P. Juilland, A. Kumar, E. Gallucci, R. J. Flatt, K. L. Scrivener, Effect of mixing on the early hydration of alite and OPC systems. Cem. Concr. Res. 42 (12) 1175-1188.
[37] C. Gay, F. Sanchez, Performance of Carbon Nanofiber – Cement Composites with a High-Range, Water Reducer (2010) 109–113, https://doi.org/10.3141/2142-16.
[38] O. Mendoza, G. Sierra, J.I. Tobón, Effect of the reagglomeration process of multi-walled carbon nanotubes dispersions on the early activity of nanosilica in cement composites, Constr. Build. Mater. 54 (2014) 550–557.
[39] P. Sudharshan Phani, W.C. Oliver, A critical assessment of the effect of indentation spacing on the measurement of hardness and modulus using instrumented indentation testing, Mater. Des. 164 (2019) 107563, , https://doi.org/10.1016/j.matdes.2018.107563.
[40] M. Vandamme, The Nanogranular Origin of Concrete Creep: A Nanoindentation Investigation of Microstructure and Fundamental Properties of Calcium-Silicate-Hydrates, Environ. Eng. 366 (2008).
[41] W.C. Oliver, G.M. Pharr, An improved technique for determining hardness and elastic modulus using load and displacement sensing indentation experiments, J. Mater. Res. 7 (1992) 1564–1583, https://doi.org/10.1557/JMR.1992.1564.
[42] L.A. Galin, I.N. Sneddon, I.N. Sneddon, Contact problems in theory of elasticity, North Carolina State College, 1961 (translated by H. Moss).
[43] I.N. Sneddon, The relation between load and penetration in the axi-symmetric Boussinesq problem for a punch of arbitrary profile, Int. J. Eng. Sci. 3 (1965) 45–57.
[44] L. Sorelli, G. Constantinides, F.J. Ulm, F. Toutlemonde, The nano-mechanical signature of Ultra High Performance Concrete by statistical nanoindentation techniques, Cem. Concr. Res. 38 (2008) 1447–1456, https://doi.org/10.1016/j.cemconres.2008.09.002.
[45] F.J. Ulm, G. Constantinides, F.H. Heukamp, Is concrete a poromechanics material? - A multiscale investigation of poroelastic properties, Mater. Struct. Constr. 37 (2004) 43–58.
[46] H.M. Jennings, Model for the microstructure of calcium silicate hydrate in cement paste, Cem. Concr. Res. 30 (2000) 101–116, https://doi.org/10.1016/S0008-8846(99)00209-4.
[47] H.M. Jennings, J.J. Thomas, J.S. Gevrenov, G. Constantinides, F.J. Ulm, A multi-technique investigation of the nanoporosity of cement paste, Cem. Concr. Res. 37 (2007) 329–336, https://doi.org/10.1016/j.cemconres.2006.03.021.
[48] G. Constantinides, F.J. Ulm, The effect of two types of C-S-H on the elasticity of cement-based materials: Results from nanoindentation and micromechanical modeling, Cem. Concr. Res. 34 (2004) 67–80, https://doi.org/10.1016/S0008-8846(03)00230-8.
[49] A.-T. Akono, N.X. Randall, F.-J. Ulm, Experimental determination of the fracture toughness via microscratch tests: Application to polymers, ceramics and metals, Mat. Res. Soc. 27 (2012) 485–493, https://doi.org/10.1557/jmr.2011.402.
[50] A.T. Akono, F.J. Ulm, An improved technique for characterizing the fracture toughness via scratch test experiments, Wear 313 (2014) 117–124, https://doi.org/10.1016/j.wear.2014.02.015.
[51] A.-T. Akono, Energetic Size Effect Law at the Microscopic Scale: Application to Progressive-load Scratch Testing, ASCE's Journal of Nanomechanics and Micromechanics (2015), https://doi.org/10.1061/(ASCE)NM.2153-5477.0000105.
[52] A.T. Akono, P.M. Reis, F.J. Ulm, Scratching as a fracture process: From butter to steel, Phys. Rev. Lett. 106 (2011) 2–5, https://doi.org/10.1103/PhysRevLett.106.204302.
[53] A.T. Akono, Y. Cui, A. Kataruka, K. Anderson, P. Kabir, Intrinsic mechanical properties of calcium aluminate crystals via the linear comparison composite method coupled with nano-indentation, Mech. Mater. 118 (2018) 74–84, https://doi.org/10.1016/j.mechmat.2017.12.007.
[54] P. Mondal, S.P. Shah, L. Marks, A reliable technique to determine the local mechanical properties at the nanoscale for cementitious materials, Cem. Concr. Res. 37 (2007) 1440–1444, https://doi.org/10.1016/j.cemconres.2007.07.001.
[55] G. Constantinides, K.S. Ravi Chandran, F.J. Ulm, K.J. Van Vliet, Grid indentation analysis of composite microstructure and mechanics: Principles and validation, Mater. Sci. Eng. A. 430 (2006) 189–202, https://doi.org/10.1016/j.msea.2006.05.125 %not add 0215.
[56] P. Mondal, Nanomechanical Properties of Cementitious Materials, Civ. Environ. Eng. 185 (2008) PhD.
[57] L. Brown, P.G. Allison, F. Sanchez, Use of nanoindentation phase characterization and homogenization to estimate the elastic modulus of heterogeneously decalcified cement pastes, Mater. Des. 142 (2018) 308–318, https://doi.org/10.1016/j.matdes.2018.01.030.
[58] F.J. Ulm, M. Vandamme, C. Bobko, J. Alberto Ortega, K. Tai, C. Ortiz, Statistical indentation techniques for hydrated nanocomposites: Concrete, bone, and shale, J. Am. Ceram. Soc. 90 (2007) 2677–2692, https://doi.org/10.1111/j.1551-2916.2007.02012.x.
[59] P.K. Mehta, Scanning electron micrographic studies of ettringite formation, Cem. Concr. Res. 6 (2) (1976) 169–182.
[60] B. Cotterell, Y.W. Mai, Crack growth resistance curve and size effect in the fracture of cement paste, J. Mater. Sci. 22 (8) (1987) 2734–2738.
[61] X. Hu, F. Wittmann, Size effect on toughness induced by crack close to free surface, Eng. Fract. Mech. 65 (2-3) (2000) 209–221.
[62] M.J. DeJong, F.J. Ulm, The nanogranular behavior of C-S-H at elevated temperatures (up to 700 C), Cem. Concr. Res. 37 (1) (2007) 1–12.
[63] J.P. Ollivier, Contribution a l'etude de L'hydratation de la pte de ciment Port- land au Voisinage des Granulats, Thesis Toulouse (1981).
[64] P.J.M. Monteiro, J.C. Maso, J.P. Ollivier, Particle Size Analysis of the Sand, Cem. Concr. Res. 15 (1985) 953–958.
[65] G. Arliguie, J. Grandet, J.P. Ollivier, Orientation de la portlandite dans les mortiers et bétons de ciment Portland: Influence de la nature et de l'état de surface du support de cristallisation, Mater. Struct. 18 (1985) 263–267, https://doi.org/10.1007/BF02472914.
[66] P. Ballester, A. Hidalgo, I. Mármol, J. Morales, L. Sánchez, Effect of brief heat-curing on microstructure and mechanical properties in fresh cement based mortars, Cem. Concr. Res. 39 (2009) 573–579, https://doi.org/10.1016/j.cemconres.2009.04.002.

[67] T. Nochaiya, A. Chaipanich, Behavior of multi-walled carbon nanotubes on the porosity and microstructure of cement-based materials, Appl. Surf. Sci. 257 (2011) 1941–1945, https://doi.org/10.1016/j.apsusc.2010.09.030.
[68] Kang Su-Tae, Seo Jun-Yeong, Park Sum-Hong, The characteristics of CNT/cement composites with acid-treated MWCNTs, Adv. Mater. Sci. Eng. (2015) 1–9 https://doi.org/10.1155/2015/308725.
[69] H.M. Jennings, Colloid model of C-S-H and implications to the problem of creep and shrinkage, Mater. Struct. 37 (1) (2004) 59–70.
[70] P. Stynoski, P. Mondal, C. Marsh, Effects of silica additives on fracture properties of carbon nanotube and carbon fiber reinforced Portland cement mortar, Cem. Concr. Compos. 55 (2015) 232–240, https://doi.org/10.1016/j.cemconcomp.2014.08.005.
[71] F. Torabian, W. Li, E. Redaelli, Dispersion of multi-walled carbon nanotubes and its effects on the properties of cement composites, Cem. Concr. Compos. 74 (2016) 154–163, https://doi.org/10.1016/j.cemconcomp.2016.09.007.
[72] R.K.A. Al-Rub, A.I. Ashour, B.M. Tyson, On the aspect ratio effect of multi-walled carbon nanotube reinforcements on the mechanical properties of cementitious nanocomposites, Constr. Build. Mater. 35 (2012) 647–655.
[73] B. Fakhim, A. Hassani, A. Rashidi, P. Ghodousi, Preparation and microstructural properties study on cement composites reinforced with multi-walled carbon nanotubes, J. Compos. Mater. 49 (1) (2015) 85–98.
[74] E.E. Gdoutos, M.S. Konsta-Gdoutos, P.A. Danoglidis, Portland cement mortar nanocomposites at low carbon nanotube and carbon nanofiber content: A fracture mechanics experimental study, Cem. Concr. Compos. 70 (2016) 110–118, https://doi.org/10.1016/j.cemconcomp.2016.03.010.
[75] A. Carriço, J.A. Bogas, A. Hawreen, M. Guedes, Durability of multi-walled carbon nanotube reinforced concrete, Constr. Build. Mater. 164 (2018) 121–133.
[76] H.M. Jennings, Refinements to colloid model of CSH in cement: CM-II, Cem. Concr. Res. 38 (3) (2008) 275–289.
[77] B. Pradhan, M. Nagesh, B. Bhattacharjee, Prediction of the hydraulic diffusivity from pore size distribution of concrete, Cem. Concr. Res. 35 (9) (2005) 1724–1733.